Injection characteristics study of high-pressure direct injector for Compressed Natural Gas (CNG) using experimental and analytical method

IOP Conf. Series: Materials Science and Engineering **257** (2017) 012057 doi:10.1088/1757-899X/257/1/012057

Injection characteristics study of high-pressure direct injector for Compressed Natural Gas (CNG) using experimental and analytical method

Z Taha[1], MF Abdul Rahim [2,3*] and R Mamat[3]

[1,2]Innovative Manufacturing and Mechatronics and Sports (IMAMS) Laboratory, Faculty of Manufacturing Engineering, Universiti Malaysia Pahang, Pahang, Malaysia.
[3]Faculty of Mechanical Engineering, Universiti Malaysia Pahang, Pahang, Malaysia

*Corresponding author: mfadzil@ump.edu.my

Abstract. The injection characteristics of direct injector affect the mixture formation and combustion processes. In addition, the injector is converted from gasoline operation for CNG application. Thus measurement of CNG direct injector mass flow rate was done by independently tested a single injector on a test bench. The first case investigated the effect of CNG injection pressure and the second case evaluate the effect of pulse-width of injection duration. An analytical model was also developed to predict the mass flow rate of the injector. The injector was operated in a choked condition in both the experiments and simulation studies. In case 1, it was shown that mass flow rate through the injector is affected by injection pressure linearly. Based on the tested injection pressure of 20 bar to 60 bar, the resultant mass flow rate are in the range of 0.4 g/s to 1.2 g/s which are met with theoretical flow rate required by the engine. However, in Case 2, it was demonstrated that the average mass flow rate at short injection durations is lower than recorded in Case 1. At injection pressure of 50 bar, the average mass flow rate for Case 2 and Case 1 are 0.7 g/s and 1.1 g/s respectively. Also, the measured mass flow rate at short injection duration showing a fluctuating data in the range of 0.2 g/s – 1.3 g/s without any noticeable trends. The injector model able to predict the trend of the mass flow rate at different injection pressure but unable to track the fluctuating trend at short injection duration.

1. Introduction

Emission produced by internal combustion engine running on conventional fossil fuels are of major concern nowadays and have become major research topic. Vehicle manufacturers are imposed by more stringent emission regulation year by year. One of the most established approaches is converting conventional fossil fuels to cleaner alternatives. The most widely accepted alternative to gasoline and diesel is compressed natural gas (CNG). Significant advantages of CNG are large proven reserves, cleaner combustion and competitive market price [1] CNG also has a higher RON number compared to gasoline and diesel hence promoting better knock resistance [2] and higher hydrogen to carbon ratio [3] therefore making it suitable as a transportation fuel. Previous studies have concluded that the power loss of CNG engine can be compensated by the use of direct injection CNG fuel system [4].

Based on previous studies, it is obvious that the application of CNG is mostly restricted to the framework of compression ignition engine. It is understood that the compression ignition engine is preferable due to their higher compression ratio which can exploit the higher knock resistance of CNG fuel. This will lead to a higher engine thermal efficiency. As an overview, in the framework of

compression ignition engine, the studies on the jet structure have been performed experimentally and numerically by [5], [6], and [7]. Other studies focus on the injection system [8] and [9], combustion development and engine emission levels [10]. Chiodi et al. [11] and Muhammad et al. [12] investigated the methane injection spray structure using Laser Induced Fluorescent (LIF) technology. The axial and radial penetration length of methane issued from multi-hole injector were measured. Chiodi et al. study was based on a multi-hole injector design whereas Muhammad et al. used an innovative spark-plug fuel injector design. Chan et al. investigated the distribution of natural gas in a partially stratified charge engine using a modified injector [13].

The previous study had also investigated the transient injection of helium and hydrogen through multi-hole gaseous injectors using Schlieren visualisation [14]. Chitsaz and Hajialimohammadi investigated the jet structure of helium injected through different nozzle diameters experimentally [15] and [16]. Both had present a correlation of tip penetration for both near and far field regions of the jet. The study on tip penetration of gaseous jets was also conducted by [17], [18], [19], and [20]. They reported different correlations for tip penetration of gaseous jets. Chitsaz et al proposed a semi-analytical solution for the transient start of a under-expanded jet using numerical Laplace transform.[20]. The injection system for the compression ignition engine has been studied in detail by [21], [6], [7], [8] and [9]. However, the major difference between previous studies and natural gas spark ignition engine is the pressure ratios of the injection and the jet structure. Also, the injection pressure of CNG in compression ignition engines is higher than those based on spark ignition engines [21] and [6] by almost two times.

The CNG application in the context of the spark ignition engine is mostly based on the multi-point port injection approach. Comparison of carburetted gasoline, port injected gasoline and direct injected gasoline has been performed by Kalam and Masjuki [4]. It is important to note that the results obtained showed that the maximum power of CNG-DI is only 5% lower than the performance of gasoline port injection. It is expected that by performing strategic optimization on the CNG-DI engine, the resulted performance can be at least at the same par with gasoline port injection engine. Commercialized CNG direct injector is hardly found in the market. Thus a commercial GDI injector is mostly used to inject CNG. The changes of fuel properties from liquid to gases affect the injector characteristic benchmarked by the manufacturer. This is the utmost important reason on why the injector characterization for the natural gas engine is highly desirable.

Conventional fuel injectors are mostly used solenoid drive unit. The electrical energy is converted to mechanical energy in term of pintle displacement via electromagnetic principle. The movement of the pintle defines the opening and closing of the nozzle which in fact controlled the fuel flow through the nozzle. The pintle movement and corresponding time scale are used to define the temporal characteristics of an injector. The temporal characteristics of an injector include injection duration, rate shape, opening delay time and closing delay time. The temporal characteristics of the injector are controlled by the ECU based on sensors data and predefined optimal setting stored in the base maps of the ECU. Sensors data are such as engine rotational speed, manifold absolute pressure, engine operating temperature, and air to fuel ratio are used by the ECU to select the corresponding optimal values for injector parameters. The ECU will send a control signal to the fuel injector power driver which instantly provide proper excitation to the solenoid to generate magnetic force. The induced magnetic force will pull the pintle to produce nozzle flow area.

The linear displacement of injector's pintle is an important variable for injector control. However, the pintle's linear displacement is affected by numbers of associated parameters which physically interacted with the pintle or armature body. The displacement occurs only when the magnetic force overcomes the opposing forces. The opposing forces are composed of inertia force, contact friction force, gas pressure force and spring compression force. Therefore, the physics involved in fuel injector operation is an interaction of electromagnetic, mechanical dynamic and fluid dynamics. High-performance injector required that pintle dynamics should have the following characteristics: (1) quick response, (2) repeatability, and (3) least power consumption [22]. Short opening delay and short closing delay are characteristics of a quick response injector. As the engine cycle completed on a scale of milliseconds, these are very crucial parameters for engine control nowadays. The fuel injection

process must be completed efficiently in a very small interval at each engine cycle. The opening and closing delay affect the minimum total time for injection duration and injection timing. Actual mass injected in a very short injection duration might not resemble theoretical values. The pintle response is also a decisive factor for multiple injections strategy. By using such approach, multiple injections must be performed in each cycle. The pintle needed to open and close at a higher frequency. Repeatable fuel injection allows a lessen fuel injection quantity and injection rate per shot but the total mass injected at each cycle is expected to be greater than a single injection approach. Moreover, it is anticipated that a less shot-to-shot variations injection quantity is produced.

Injector current affects the response of the pintle. In general, current is load dependent. The higher the resistance to pintle movement (gas pressure, friction, spring forces), then higher current shall be withdrawn from the power supply to overcome the load. Higher current may as well ensure the repeatability of the injection by creating more than enough magnetic force to hold the pintle at its desired position. Insufficient current supply may cause the pintle partially pulled and vibrated during the opening and closing of the injector. Increasing the current ramp rate theoretically will reduce the opening delay and closing delay. However, in practical, the current increment rate is influenced by the inductance of the solenoid. Also, the higher current would create more heat in the solenoid, which increases the temperature of the surrounding magnetic material. The increased heat of the magnetic material will deteriorate the magnetic material properties. Among the distressed magnetic properties are lowered saturation limit and increased hysteresis. The deterioration of these properties will distract the pintle response time. Other factors affecting the pintle response time are hydraulic hysteresis, magnetization hysteresis and saturation of the magnetic material.

Earlier discussions have focused mainly on the experimental characterization of injectors. The studies of direct injector were also explored using modelling approaches. The modelling of injectors had extended from the injector physical modelling until complete injection system modelling. The direct injectors were mainly modelled using an analytical approach. The extent of models can be categorized into two major areas which are (1) injector dynamics modelling and (2) power driver design and optimization. The numerical models usually include or partially include coupled multi-physics problem [23-25]. Major components of a model are an electromagnetic model, the mechanical/ dynamic model, and the dynamic flow model. A model coupled one-dimensional hydraulics with a two-dimensional (2D) axisymmetric electromagnetic finite element code has been developed by Digesu to calculate the magnetic force regarding exciting current and working gap [26]. He validated simulated results of needle lift, pressures (pipes, control volume, rail and accumulative volume) and flow rate with experimental data. He had demonstrated the effect of pipe design on the needle lift profile due to the hydraulic wave. Ficarella had evaluated the instability phenomena in a common rail injection system using numerical modelling. He had also used the model for predicting injection characteristics [27]. He concluded that the control valve residual motion had caused re-opening of the valve after a pilot injection and was considered as the most challenging part of the modelling.

Coppo's had developed a model of a common-rail injector with a combined pipe, fluid, mechanical and electromagnetic model [24, 25]. He experimentally measured exciting current signals as the input to the model which included magnetic saturation effects. Good agreement was observed between calculated and experimental profiles of rail pressure, needle lift, and injection quantity. Hu model excluded the used of electromagnetic sub-model. Instead, a measured magnetic force profile is used as the input to the model's calculation. His model was able to correlate the pressure profile with the measured one [28]. Ando developed a one-dimensional injector model which coupled the electromagnetic model with simplified rigid body and fluid models [29]. Ando used the model to study the electromagnetic effects including magnetization time lag.

The power driver is the interim unit between injectors and ECU which manage the power supplied to the injector. The power driver is essential to drive the injector operation at their optimum and designed condition. Tsai had developed a power driver for high-pressure gasoline direct injectors (GDI). The injector is a peak and holds injector, and the proposed power driver by Tsai was a three-stage power driver. The first two stages of the driver used a power Metal-Oxide-Semiconductor Field-

Effect Transistor (MOSFET) to switch between power supplies. While the 3rd stage used pulse-width-modulation (PWM) control. The results showed that the pintle closed faster with the 3rd stage PWM control than with a direct voltage control method [30]. Tsai had also performed a parametric study to investigate the effect of voltage, current, frequency and fuel pressure on injection quantity.

From the literature review, it was found out that the previous studies on direct fuel injector were very crucial, but the characterization study was mostly centred on the application of conventional fuel such as gasoline and diesel. The characterization of a direct fuel injector for natural gas is rarely found. The characteristics of direct injection CNG affects the overall engine performance. Therefore it is very crucial to investigate the injection characteristics, fuel metering, design and optimization of such system. Hence, this study is conducted to analyze the fuel metering of direct injector used for CNG fueling. This is to confirm the sufficiency of the fuel supplied to the engine requirement throughout the engine operating regime. The work of Erfan et al. [31], and Chitsaz et al. [15] are among the significant work concentrated on the direct fuel injector characterization for CNG. However, their work only used experimental approach. In this study, the characterization was also utilized modelling approach. The injector dynamic-analytical model is vital for detail cause-effect relationship studies and able to be coupled with analytical engine models for the development of a fully predictive engine model. The method of the modelling is using electromagnetic model coupled with mechanical and fluid flow model.

2. Experimental apparatus

The physical layout of the baseline injector is shown by figure 1(a). The injector is a Bosch HDEV 1.2 injector for gasoline direct injection (GDI) engine. General specification of the injector and flow characteristics for gasoline fuel operation is provided in table 1. The maximum allowable fuel pressure for the injector is 200 bar. Calibration of the injector with gasoline fuel at 100 bar produced an estimated volumetric flow rate of 30 cm3/min or 0.36 g/s (by taking gasoline density as 719.7 kg/m^3). In this study, the fuel pressure was regulated in between 20 bar to 60 bar. The mass flow rate for different pressure and injection duration are to be determined. Conversion of the injector for running on CNG is studied in this paper using an experimental and modelling approach. The main injector's components consist of an armature, return spring, fine fuel filter, solenoid driver, and nozzle tip. The arrangement of components is shown in figure 1(b). Based on the injector construction, the injector armature is pulled backwards as the solenoid is energized causing the nozzle pintle lift up and the nozzle flow area opened. As the solenoid is de-energized, the return spring pushes the pintle back to its seat, closing the nozzle flow area.

The experimental setup is shown schematically in figure 2**.** This setup comprises of a CNG supply tank, fuel pressure regulator, pressure gauge, test injector, injector micro controller, and a control computer. The microcontroller act as a pulse generator, provides square wave signals with adjustable frequency and amplitude to a PWM driver who drive the injector in different modes. A digital scale is used to record the instantaneous cylinder mass tanks after some injection is completed. The mass changes is used to determine the mass flow rate of the injector. The time factor is calculated by the total length of the “on” signals produced by the microcontroller. In the experiment, a constant 12 V supply is provided through the PWM driver. The supply current is limited to 8 Amp to replicate the saturated current limit used in the actual electronic control unit (ECU) of the prototype vehicle.

Table 1. General injector specification, model HDEV 1.2.

Attributes	Values
Mechanical specifications	
Allowable maximum pressure (bar)	200
Volume flow rate (gasoline fuel/cm3/min) at 100 bar	30
Weight (g)	78
Length (mm)	85
Electrical specifications	
Resistance (Ohm)	0.9 @ 1.5
Voltage (Volt)	90 V
Allowable peak current (Amp)	20 A
Operating Condition (Gasoline fuel)	
Fuel Input	Axial (top feed)
Operating Temperatures (^{o}C)	30-120
Permissible Fuel Temperatures (^{o}C)	<80

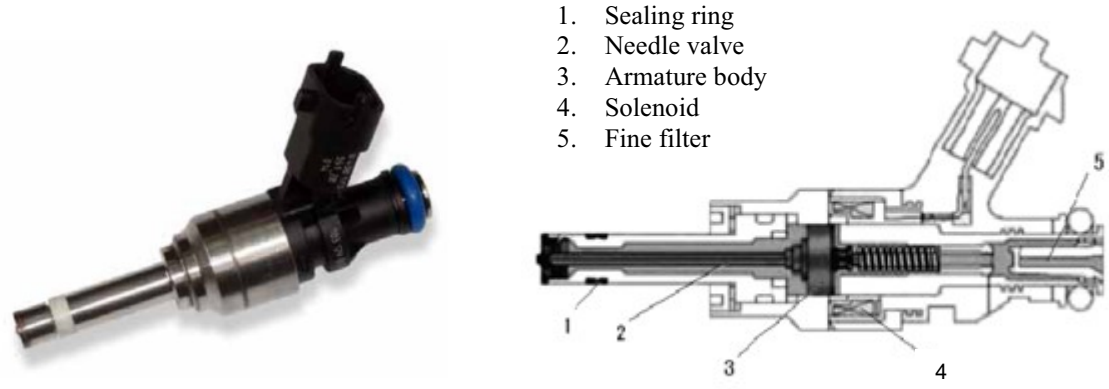

(a) (b)

Figure 1(a). Photo of injector physical appearance and (b) Injector cut-view of Bosch single-hole gasoline direct injector [30].

3. Experimental procedures

The varied parameters in this study are the injection pressure and the injection duration. In Case 1, the injection pressure is varied from 20-60 bar with an increment of 20 bar. At each pressure setting, the CNG fuel is injected at a 25 ms duration from 0 to 3000 injection count with an increment of 100 counts per step. The fuel is injected into ambient condition concerning the actual HPDI-CNG system which is utilized in a vehicle prototype. The ambient condition is assumed to be the downstream pressure because the direct injection of gas in the prototype vehicle is injected at the valve opening event. In Case 2, the injection duration is varied in the range of 2 to 26 ms. At each duration setup, the injection count is set to 500 counts.

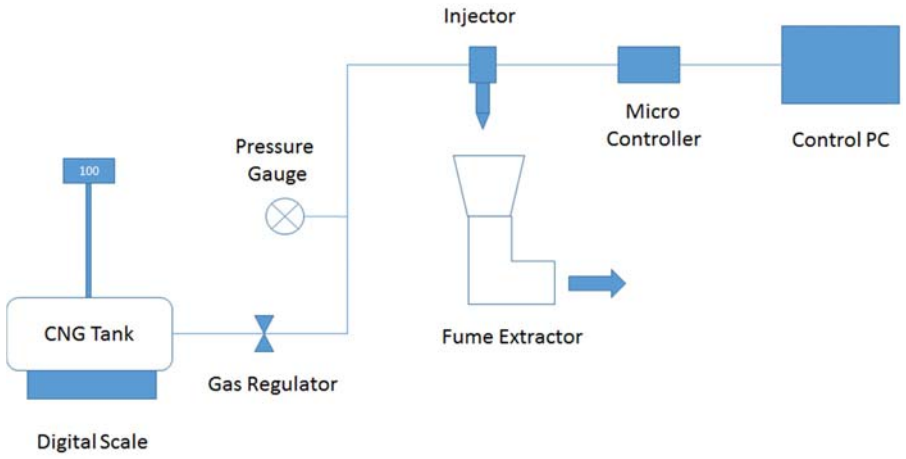

Figure 2. Schematic diagram of experimental setup.

Table 2.Experimental conditions.

Parameters (units)	Values
Number of nozzles	Single hole injector
Spray Angle (Degree)	11
Injected gas	Compressed natural gas
CNG molar mass kgkmol)	18.12
Chamber gas	Nitrogen
Chamber temperature (K)	295.5
Ambient temperature (K)	295.5
Ambient pressure (bar)	1
Injection pressure (bar) (Case 1)	20,30,40,50,60
Injection time duration (ms)	25
Varied time duration (ms) (Case 2)	2-26 (interval of 2)

4. Injector modelling approach

The modelling section is elaborated in four different section (1) The electromagnetic model, (2) the mechanical model and (3) the flow sub models. These models are combined and developed in Matlab/Simulink environment. The Matlab ODE solver is selected as the baseline solver in the study.

4.1 The electromagnetic model

The electromagnetic is based on the work of Schimpf [32]. The solenoid driver presented by Schimpf is a derivation of electromagnetic force regarding coil diameter, coil length, wire gauge, supply voltage, packing density, and the number of turns. This model eliminates the current term which in most cases are difficult to solve. Detail discussion and explanation of the model can be found in Schimpf. The electromagnetic force is given by the following expressions:

$$F_{\text{mag}} = \frac{-V^2 \mu_{\text{r}} \mu_{\text{o}}}{8\pi\gamma^2 l^2} \left(\frac{r_{\text{o}}}{r_{\text{a}}}\right)^2 \alpha e^{-\frac{\alpha}{l}x} \tag{1}$$

or

$$F_{\text{mag}} = \frac{-V^2 \mu_{\text{r}} \mu_{\text{o}}}{8\pi\gamma^2 l^2} W_{\text{f}} \alpha e^{-\frac{\alpha}{l}x} \tag{2}$$

where

V : Supply voltage
μ_r : Relative magnetic permeability of armature/pintle material
μ_o : Air gaps magnetic permeability
r_o : Inner radius of coil cross section
r_a : Average radius of coil cross section
γ : Ratio of coil material resistivity to coil wire cross section area
W_f : Winding factor, equal to square of r_o/r_a ratio
l : Length of coil body
α : Ratio of inductance to relative permeability of armature material
x : Instantaneous position of armature

To utilize the model, one needed to have detail information of the coil material. For example, the type of coil material, coil material resistivity and coil wire cross-section area. In general, the larger the coil wire cross section area, the larger the generated force. In the study, the selected coil wire is estimated to be based on AWG 43 which has a diameter of 0.07874 mm and copper type.

4.2 The mechanical model

The mechanical system of the direct injector is represented by a mass-spring-damper system. In the initial state, it was assumed that the pintle sits on the valve seats. In this initial state, a total of five forces are acting on the pintle. The gas pressure force, contact friction force, gravitational force, initial spring force, and finally normal reaction force**.** Figure 3 presents the free body diagram of the pintle in the study. The gas force is due to the CNG fuel pressure, the contact friction force is due to the contact between the pintle and surface of the valve seats, and the gravitational force is due to the mass of the pintle. The initial spring force is due to the compression of the spring at the initial state. Additional spring force will be generated as the pintle is pulled by the solenoids. The normal reaction force defines the existence of the lower (and upper) stopper of valve seats. This force is represented by the virtual spring, and damper unit which is equal and opposite direction of all other forces when the pintle rest or hit bottom and upper stopper.

The pintle act as a plunger which open and closes the nozzle flow area. During the opening state of the injector, the pintle will overcome all the resistant forces by withdrawing required current from the power supplies. The relationship between the all the forces is described by the mathematical expressions of the pintle's equation of motion which is given by equation 3. Based on the equation, the displacement of the pintle can be obtained by a twice integration of the acceleration. The mass considered in the equation is only the mass of moving the rigid body of the pintle.

$$m\cdot\ddot{x}=F_{\text{sol}}+F_{\text{spring}}+F_{\text{contact friction}}+F_{\text{upper wall}}+F_{\text{bottom wall}}+F_{\text{pressure}} \quad (3)$$

The spring compression force F_{spring} Is defined as the sum of initial compression force and the force due to the additional compression during the solenoid activation. The equation for the spring compression force is given by the following expression.

$$F_{\text{spring}}(\text{x})=F_0+K_{\text{spring}}\cdot x \quad (4)$$

where,

F_0 : the initial compression force, N
K_{spring} : spring constant, N/m

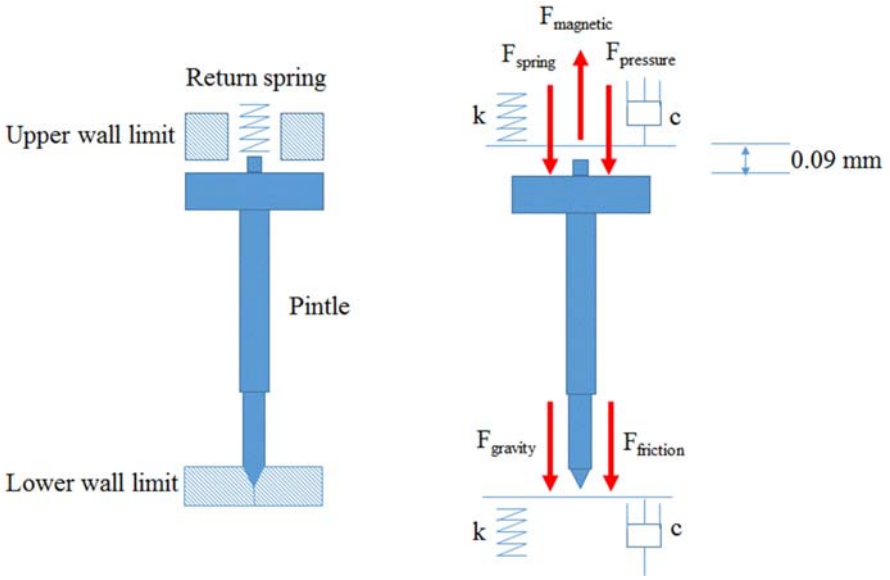

Figure 3. Pintle free body diagram.

The initial contact friction force is given a constant value of 13.8 N at its rest position (at the upper stator or lower stator). The value will reduce to zero as the position of the pintle surpassed a threshold distance of 0.001 mm. The mathematical form of the contact friction force is given by equation 5.

$$F_{\text{initial contact friction}}(x)=\begin{cases}\text{-13.8N}, & \& \ x\leq \text{1e-3mm}\\ 0, & \& \ x>\text{1e-3mm}\end{cases} \tag{5}$$

Based on the findings of Zhang et al. [22] the displacement of the pintle is limited by the existing of the bottom and upper stator. The maximum displacement allowable for the pintle is estimated to be 0.09 mm upwardly. Farther than that, a barrier is enforced by imposing a stiff spring and damper. This is to simulate a condition where the pintle hits the stator. The reaction force imposed on the pintle at the upper wall is expressed mathematically by equation 6.

$$F_{\text{upper wall}}(x)=\begin{cases}-K*(x\text{-}0.09\text{mm})-c*\dot{x}, & \&x<0\\ 0, & \&x>0\end{cases} \tag{6}$$

As the pintle moves back to the initial position and hit the lower stator, another barrier is imposed to simulate the reaction force from the bottom stator. The mathematical expression for the lower stator reaction force is given by equation 7.

$$F_{\text{bottom wall}}(\text{x})=\begin{cases}-K*x-c*\dot{x}, & x<0\\ 0, & \&x>0\end{cases} \tag{7}$$

where,

K : the wall stiffness, N/m
C : the damping coefficient, N·s/m

4.3 The flow model

The flow model is based on one-dimensional compressible flow equation. The model considers choking and non-choke flow situations which are determined by the critical pressure ratio. Choked flow occurs when the ratio P_1/P_2 exceeds the critical pressure ratioP_c, which is given by the following equation.

$$P_c = \left(\frac{\gamma+1}{2}\right)^{\frac{\gamma}{(\gamma-1)}} \tag{8}$$

The mass flow rate through the orifice for non-choked and choked flow conditions are given by equation 9 and 10 respectively. The only varying parameter in the equation 9 is the effective area of the nozzle which is calculated as a function of pintle displacement.

$$\dot{m} = K_{nv} A P_1 \sqrt{\frac{2M}{RT}\left(\frac{\gamma}{\gamma-1}\right)\left[\left(\frac{P_2}{P_1}\right)^{\frac{2}{\gamma}} - \left(\frac{P_2}{P_1}\right)^{\frac{(\gamma+1)}{\gamma}}\right]} \tag{9}$$

or

$$\dot{m} = K_{nv} A P_1 \sqrt{\frac{\gamma M}{RT}\left(\frac{2\gamma}{\gamma-1}\right)^{\frac{(\gamma+1)}{(\gamma-1)}}} \tag{10}$$

Where,

K_{nv}	: the discharge flow coefficients
A	: the orifice area (m^2)
P_1	: the H_2 upstream pressure (Pa)
P_2	: the in-cylinder pressure (Pa)
T	: the H_2 upstream temperature (K)

The crucial part of the flow model is the definition of the nozzle effective flow area. Figure 4 presents a schematic definition of the nozzle effective flow area for the pulled-in injector. The effective flow area is defined as a surface area of a truncated cone. The effective flow area is formulated based on the work of Antunes [33].

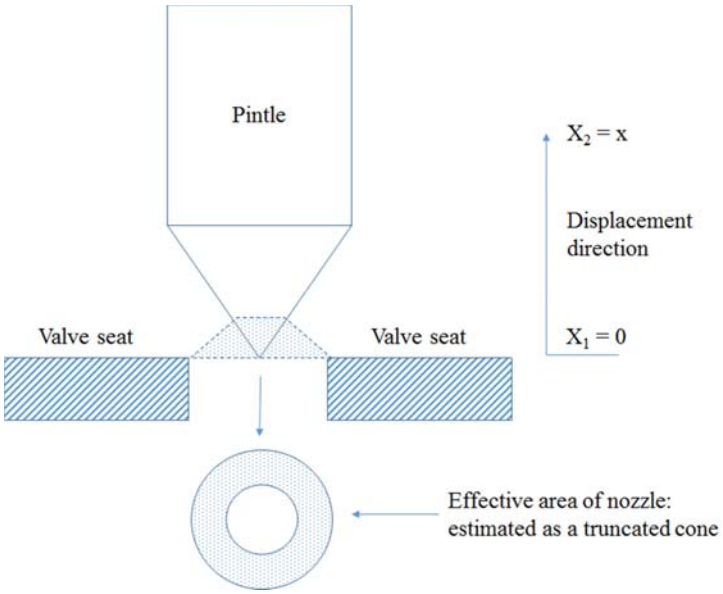

Figure 4. Definitions of effective flow area for nozzle flow calculation.
Source: Antunes [33].

In mathematical form, the effective area for the nozzle flow, as illustrated in Figure 4, can be calculated by using equation 11.

$$A_o=\pi\left[\left(R\sqrt{R^2+(R\sin\varphi)}\right)-\left(R-X\sin\varphi\sin\varphi\right)\sqrt{\left(R-X\sin\varphi\sin\varphi\right)^2+(R\tan\varphi-X\sin^2\varphi)^2}\right] \quad (11)$$

Where,

R : the nozzle hole radius (m)
θ : the needle tip angle (rad)
ϕ : is equal to $\theta/2$

The maximum area of the nozzle is given by:

$$A_{o\,Max}=\pi R^2 \quad (12)$$

5. Simulation Setup

5.1 Model Input

The simulation was carried out to replicate the two cases from the experiment. A significant amount of inputs are required to ensure the model can predict as close as possible to the measured data. Table 3 listed all the general and specific inputs required by the model.

The selected injection pressure of 50 bar is equivalent to the injection pressure used in actual prototype vehicle of CNG direct injection. The varied values are used to study the effect of injection pressure on the injected mass quantity. The electro-magnetic inputs, as well as the mechanical inputs parameter of the injector, are mostly based on Zhang et al. [22]. Figure 5 presents the layout of the simulation model developed in Matlab/Simulink. The pulse generator produced square wave signal which represents the output of the PWM driver.

6. Results and discussion

The injected mass flow rate is assumed to be equal to the rate of change of mass from the CNG storage tank. In case 1, the injector frequency and injection duration are 8 Hz and 25 ms respectively. Based on Erfan et al. [31], the injection duration should be less than 50% of the time between pulses. Therefore, in the study, the injection duration cannot exceed 50 ms at the frequency of 8 Hz. The results of figure 6(a) and 6(b) shows the example of CNG storage tank mass for injection pressure of 20 bar and 60 bar plotted against the injection time. The value of mass reduction can be approximated by a linear equation for all cases. The slope of the plot is representative of the injector mass flow rate for different injection pressure. It is noticeable that the mass flow rate is increased as the injection pressure increased. The resulting mass flow rate at different injection pressure are summarized in table 4. The trend of the results obtained is comparable to earlier results of [31].

Table 3. Simulation model input.

Attributes	Values
General Input Parameter (unit)	
Actuator radius (m)	0.005
Gas pressure (bar)	20, 30,40,50, 60
Nozzle Diameter(m)	0.00068
Spring Constant (N/m)	12140 N/m
Electro-magnetic Input Parameters (unit)	
Length of air gap (m)	0.00009
Magnetic Permeability of Air (H/m)	1.256×10^{-6}
Magnetic Permeability of Steel (H/m)	3290
Magnetic circuit length (m)	~0.001
Number of Turns	160
Coil Resistance (Ohm)	0.9
Resistance (ohm)	1.5 (Zhang)
Inductance (mH)	1.9 mH @ 1kHz 3.9 mH @0.12 kHz
Voltage (Volt)	90
Peak Current (Amps)	20
Mechanical Input Parameters (unit)	
Static Spring Force (N)	40
Spring mass (kg)	0.001
Actuator Mass (kg)	0.003
Actuator Damping Constant (Nm/s2)	14.97 N.s/m
Overall Weight (kg)	0.078
Flow Input Parameters (unit)	
Gas specific heat ratio	1.32
Gas valve flow co-efficient	0.65
Universal gas constant (J/kg.K)	8314
Gas Molecular Mass (kg/kmol)	16.04
Gas Supply Temperature (K)	300

Table 4. Case 1: Effect of injection pressure results summary.

Injection Pressure (bar)	Mass flow rate (g/s)
20	0.4
30	0.4
40	0.7
50	1.1
60	1.2

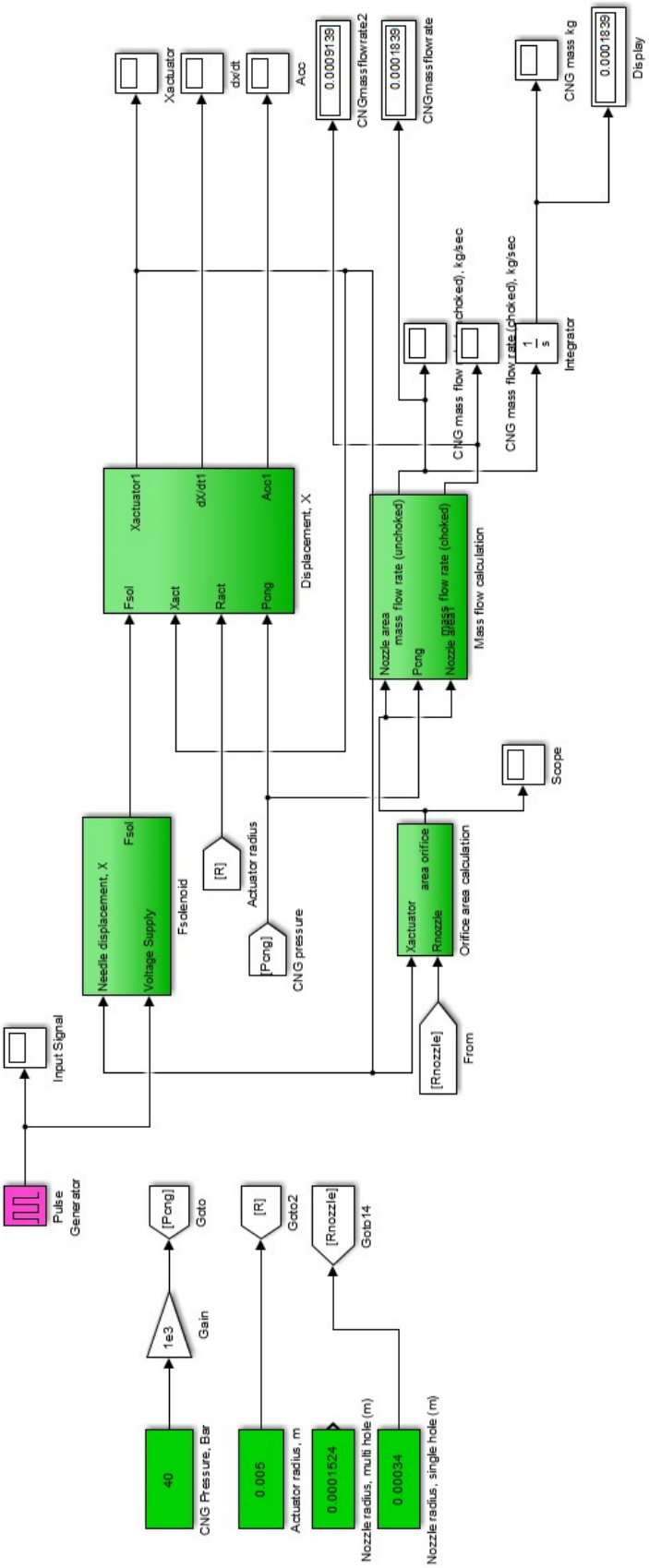

Figure 5. Matlab/Simulink model layout.

As a guideline of fuel requirement for the injector utilization in prototype CNG-DI vehicle, the mass flow rate which is needed for a conventional 1.6-liter engine have been calculated. Under stoichiometric chemical reaction for methane by assuming methane as a main composition of CNG, we have a stoichiometric air to fuel ratio for the engine of about 0.058 (or 17.24 air to fuel ratio). The required mass of fuel is proportional to the mass of air. By assuming that the engine displacement is 1.6 litre and the average volumetric efficiency of the engine is about 90%, the mass of air for stoichiometric combustion is about 0.36 g. Therefore, the required mass of fuel for stoichiometric combustion is about 0.02g. However, these requirement is also affected by the engine speed. Table 5 summarised the fuel requirement as a function of engine speed for stoichiometric combustion.

Table 5. Fuel requirement for different engine speed by assuming the fuel can be injected 300 crank angle in each cycle.

Engine speed (rpm)	Required mass flow rate (g/s)
1000	0.2
2000	0.4
3000	0.6
4000	0.8
5000	1.0
6000	1.2

Based on table 4 and table 5, the maximum requirement of fuel flow rate for a 1.6-liter engine at 6000 rpm is about 1.2 g/s while the minimum requirement is about 0.2 g/s at 1000 rpm (idle speed). By considering the effect of injection pressure, it is noteworthy that the best injection pressure which suits the engine requirement at all engine speed is 60 bar. This is the condition if the engine theoretically needs to be operated in a stoichiometric combustion. If the engine is operated at a lower injection pressure, the utmost significant effect on the engine performance is the engine will operate at a leaner mixture which will result in critical power drop, especially at high engine speed.

For Case 2, the injector is operated by varying the injection duration from 2 to 26 ms at the injection pressure of 50 bar and delay between pulses is retained at 100 ms. Therefore, as the injection duration is increased, the frequency of the injector is decreased. In this context, the frequency is defined as the number of injection per second. Based on figure 7, it is noticeable that the total mass injected will increase linearly with increased injection duration. The increased of injection duration has provided a longer delivery time for the injector. This has enabled higher amount of mass flowing through the nozzle. Figure 8 shows that the average mass flow rate of the injector is fluctuating with increased injection duration. Based on the case setup, the expected mass flow rate is about 1.1 g/s as in Case 1(p = 50 bar). However, the measured results in Case 2 possess a fluctuating trend of this variable. The maximum and minimum mass flow rates are 1.33 g/s and 0.2 g/s respectively.

The highly fluctuated mass flow rates measured at short injection duration. This indicates that, the length of injection duration is crucial in direct injection process. As the injection duration increased, the degree of fluctuation is reduced as demonstrated by Case 1. But if the injection duration is reduced as in Case 2, the consistency of the mass delivered by the injector is deteriorated. Detail study of the inconsistency of injector mass flow rate during short injection duration has never been presented previously. The results suggested that at short injection duration, the resultant mixture air to fuel ratio will fluctuate as well. This may suggest unstable combustion process due to mixture ratio inconsistency.

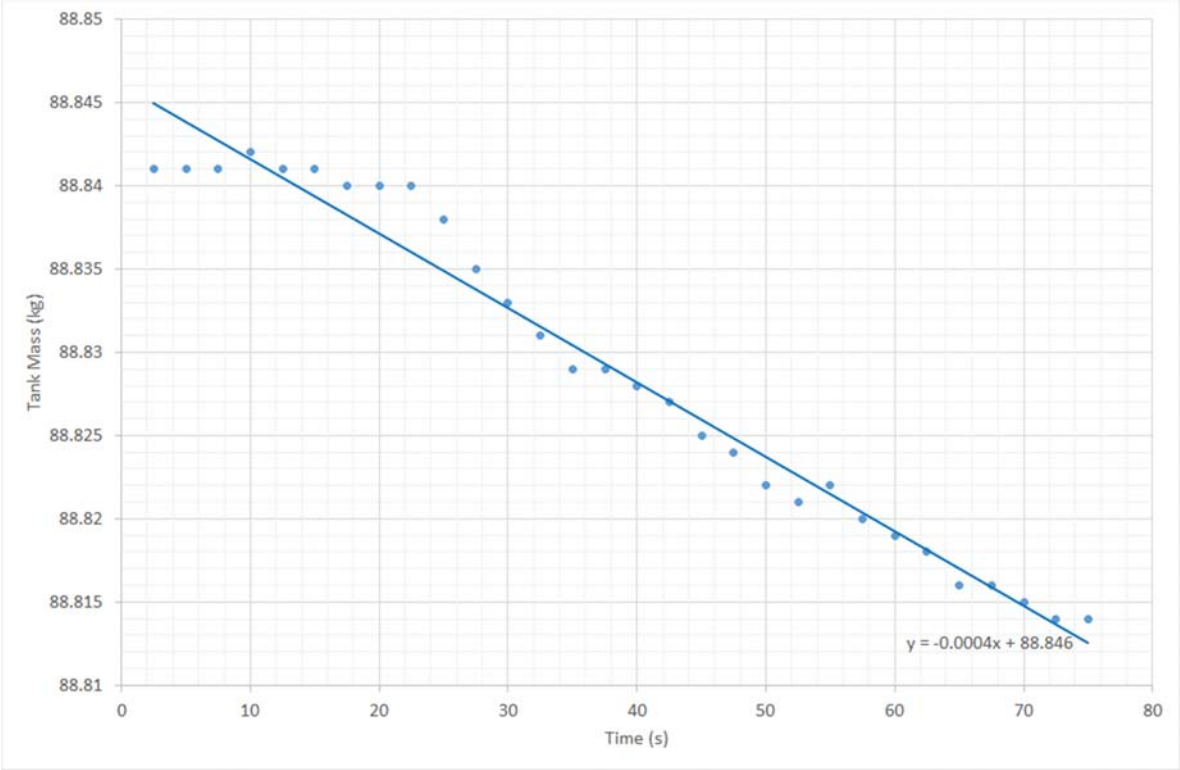

(a)

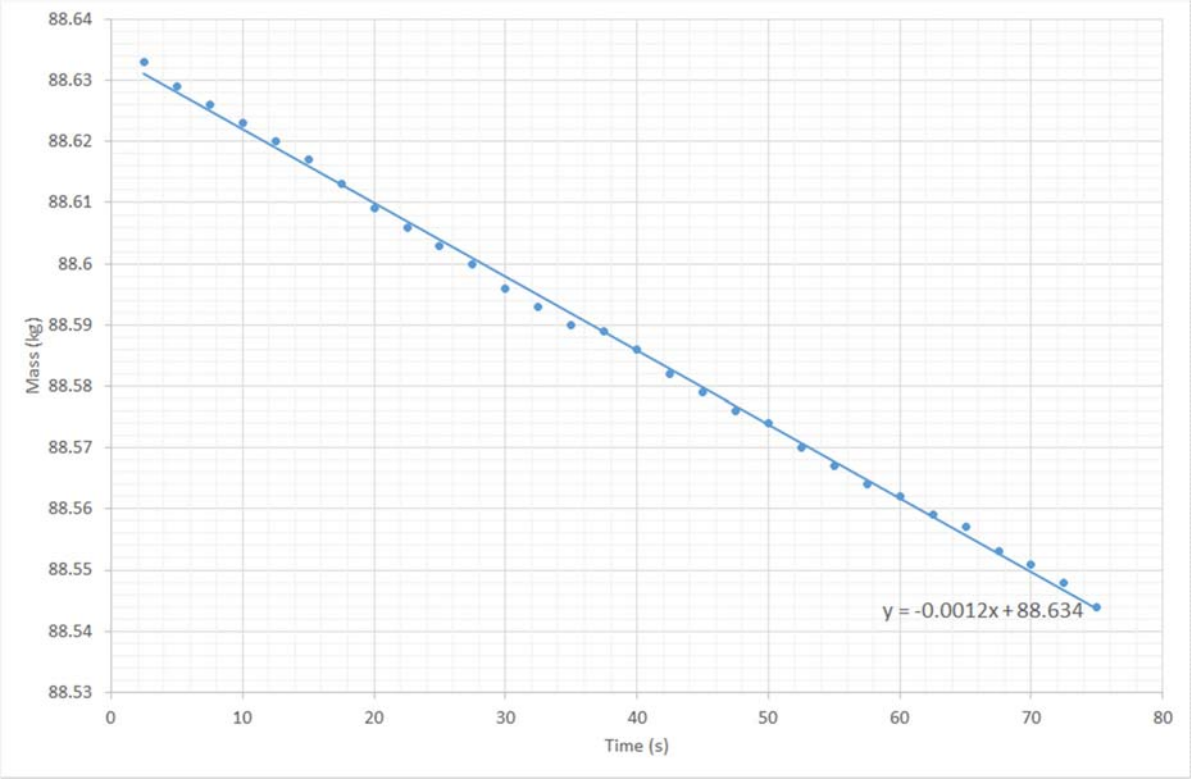

(b)

Figure 6. Instantaneous CNG storage tank mass for (a) injection pressure = 20 bar, and (b) Injection pressure = 60 bar.

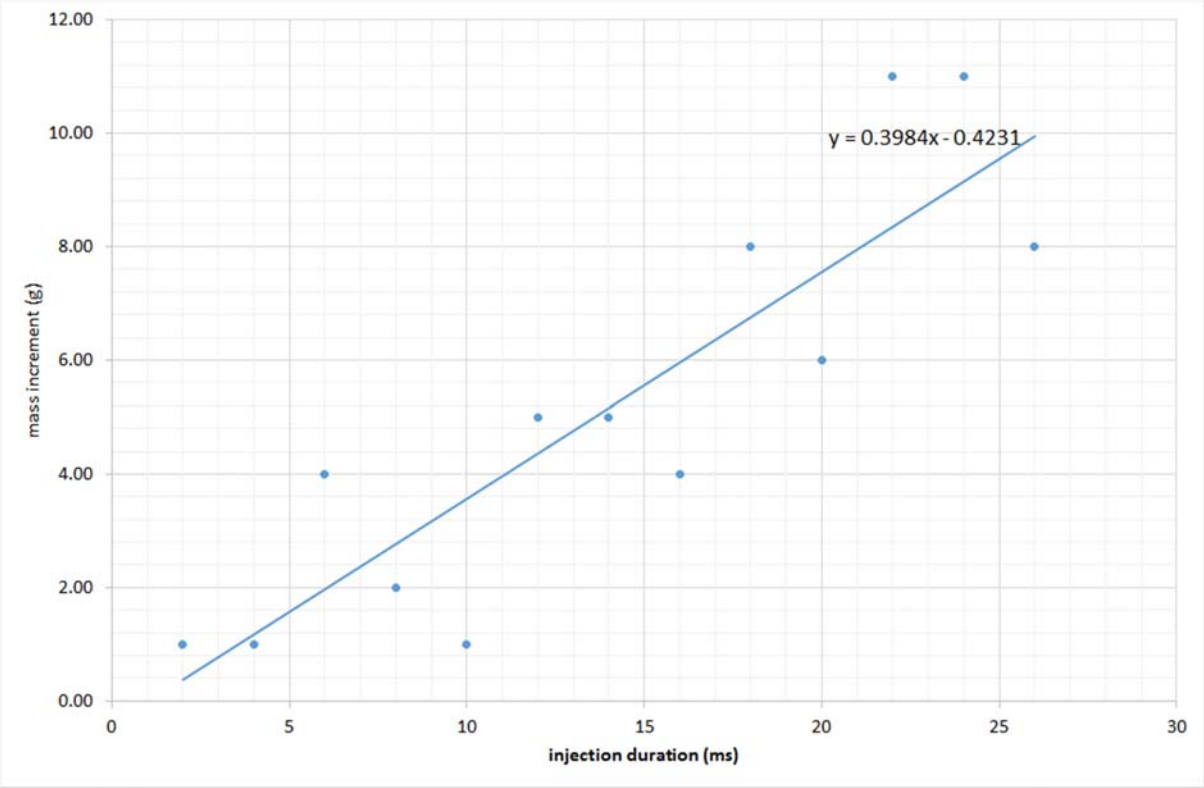

Figure 7. Mass increment at increased injection duration for Case 2.

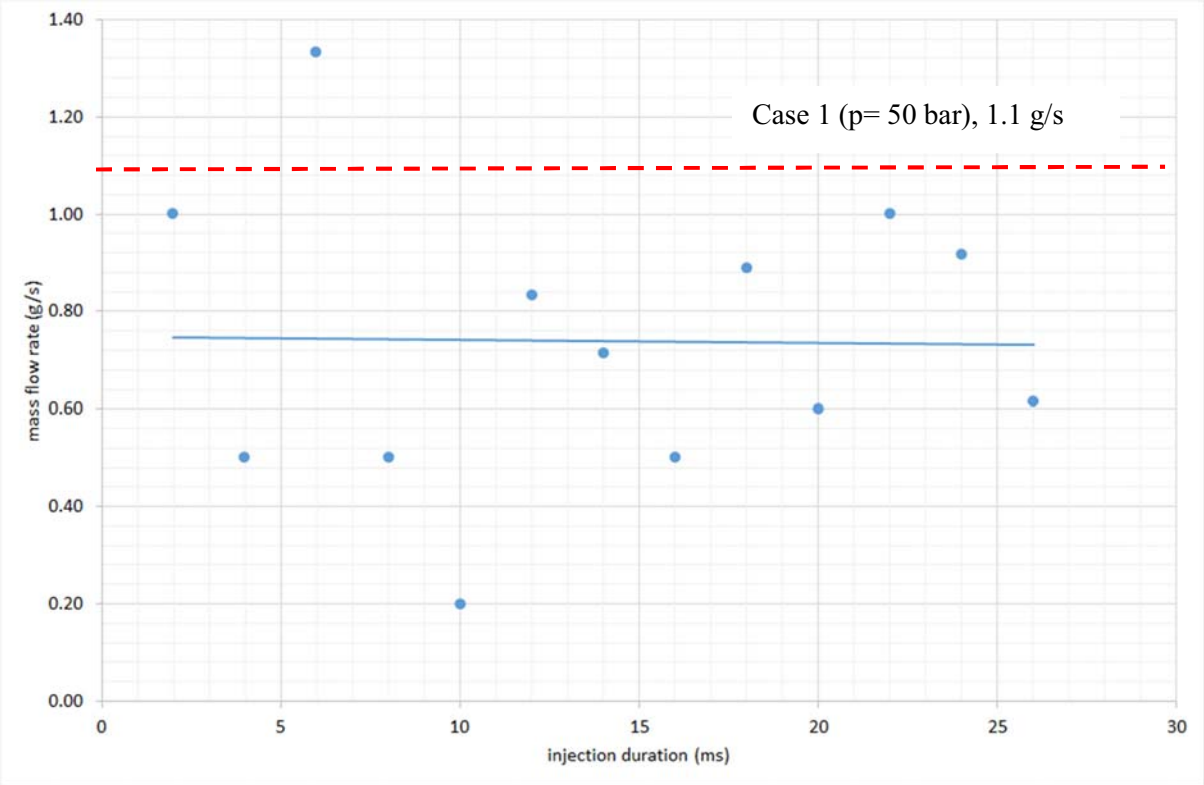

Figure 8. Mass flow rate at increased injection duration for Case 2.

The results also suggest that the frequency of the injector may affect the mass flow rate of the injector. Table 6 presents the cycle time and frequency used in Case 2. The degree of fluctuation of mass flow rates are reduced as the frequency of the injector is lowered.

Table 6. Cycle time and frequency used in Case 2.

Duration (ms)	cycle time (s)	frequency (Hz)
2	0.102	9.804
4	0.104	9.615
6	0.106	9.434
8	0.108	9.259
10	0.11	9.091
12	0.112	8.929
14	0.114	8.772
16	0.116	8.621
18	0.118	8.475
20	0.12	8.333
22	0.122	8.197
24	0.124	8.065
26	0.126	7.937

Figure 9 presents comparison of measured and simulated results for mass flow rate at different injection pressure of Case 1. The simulated mass flow rate is higher than the measured data. However, both predicts the same trend where the mass flow rate is linearly increased as the injection pressure is increased. Figure 10 presents comparison of measured and simulated mass increment for different injection duration of Case 2. The simulated mass increment is higher than the measured mass. Both the simulation and experiment predicted linear increment of mass as the injection duration increased. The rate of mass increment is higher for the simulation model compared to the experiment. Figure 11 presents comparison of measured and simulated mass flow rate at different injection duration of Case 2. Both the simulation model and experiment possess a constant trend of mass flow rate and independent of injection duration. However, the simulated mass flow rate is higher than measured results. The simulated model predict a mass flow rate of 1.06 g/s whereas the mass flow rate plot for Case 2 is about 0.75 g/s.

Based on the simulated results, it is concluded that the simulation is confirmed to be capable to predict the trend of the injector mass flow rate at different injection pressure and different injection duration. But the injector model predicted higher values of mass flow rate compared to measured results in both cases. This discrepancy is suspected due to certain properties of the model which are adapted from previous studies which may not fully suitable for the injector in current study. Detail parametric study is needed to clarify the effect of each injector parameters towards injector's mass flow rate. In addition, the theoretical calculation of the injector unable to track the fluctuating trend of mass flow rate at each injection duration. This will required detail analysis of the losses inside the injector solenoid driver and its effect on the injector opening and closing time. It is possible that at short injection duration, the opening and closing of the injector are not perfectly done due to extremely short period of cyclic operation. The simulation model is only simulate an idealized process of fuel injection.

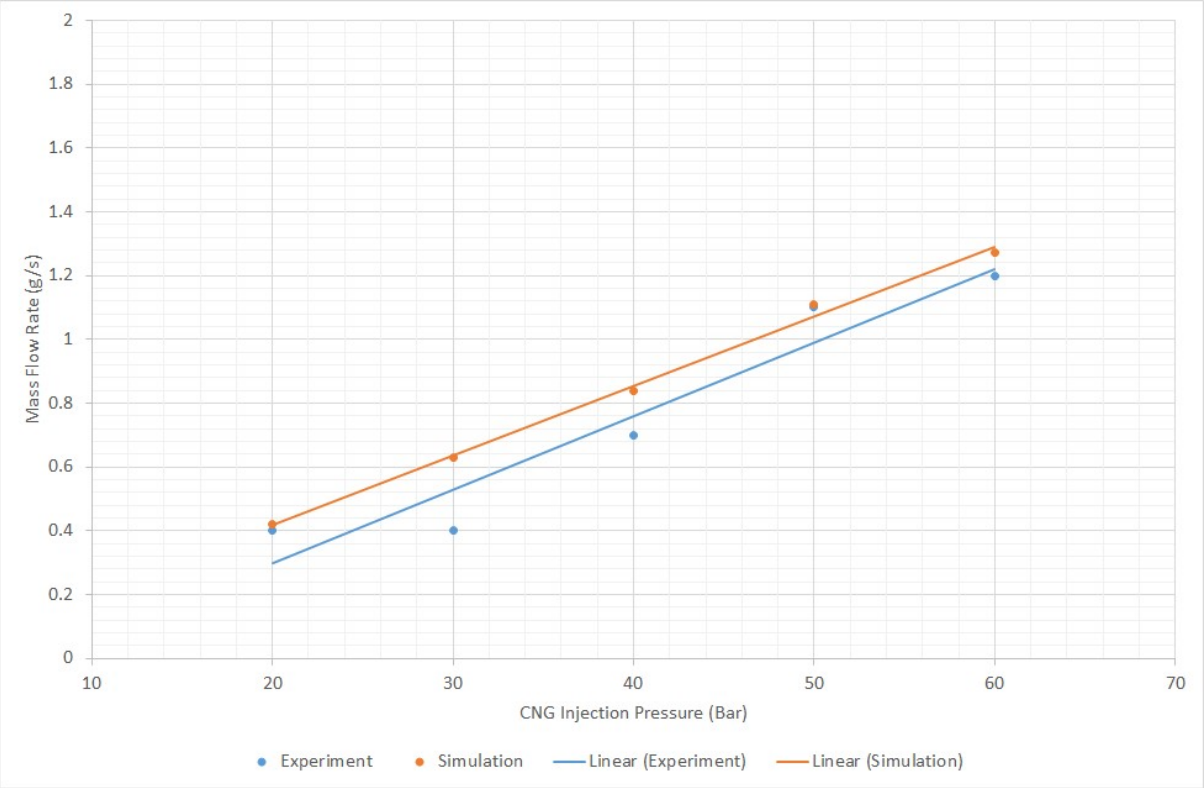

Figure 9. Comparison of simulated and measured mass flow rate for different gas injection pressure for Case 1.

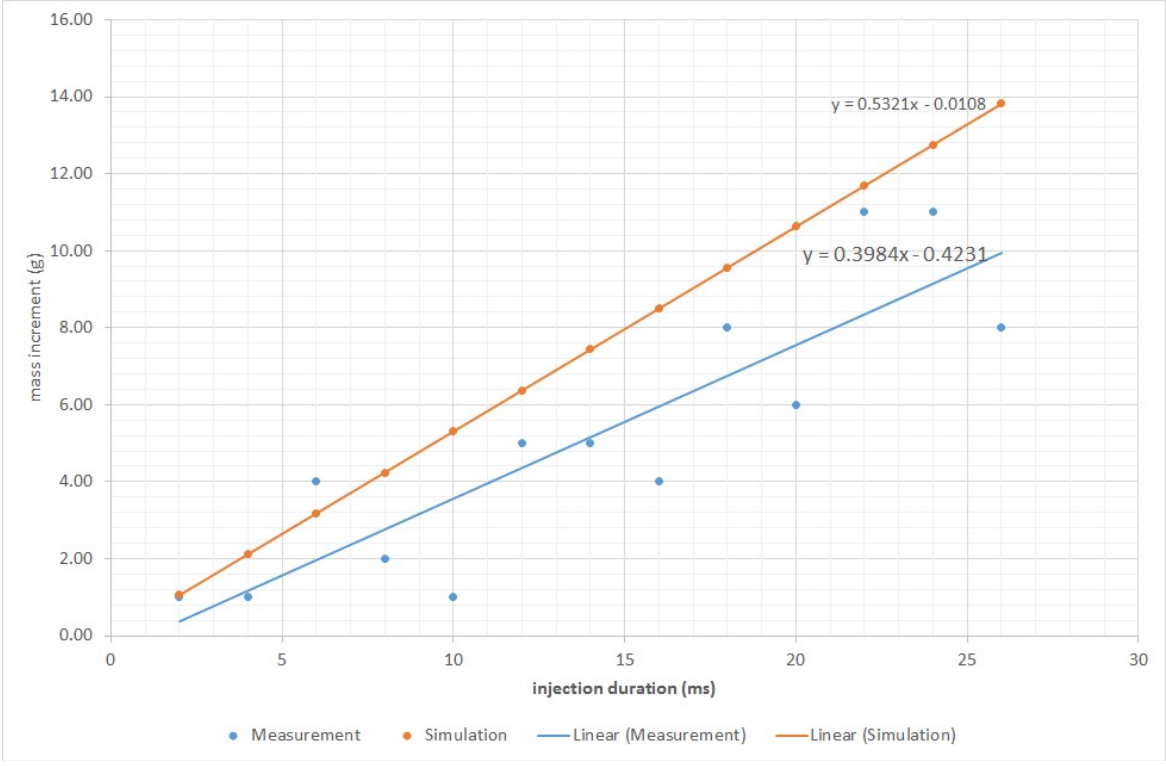

Figure 10. Comparison of measured and simulated mass increment for different injection duration for Case 2.

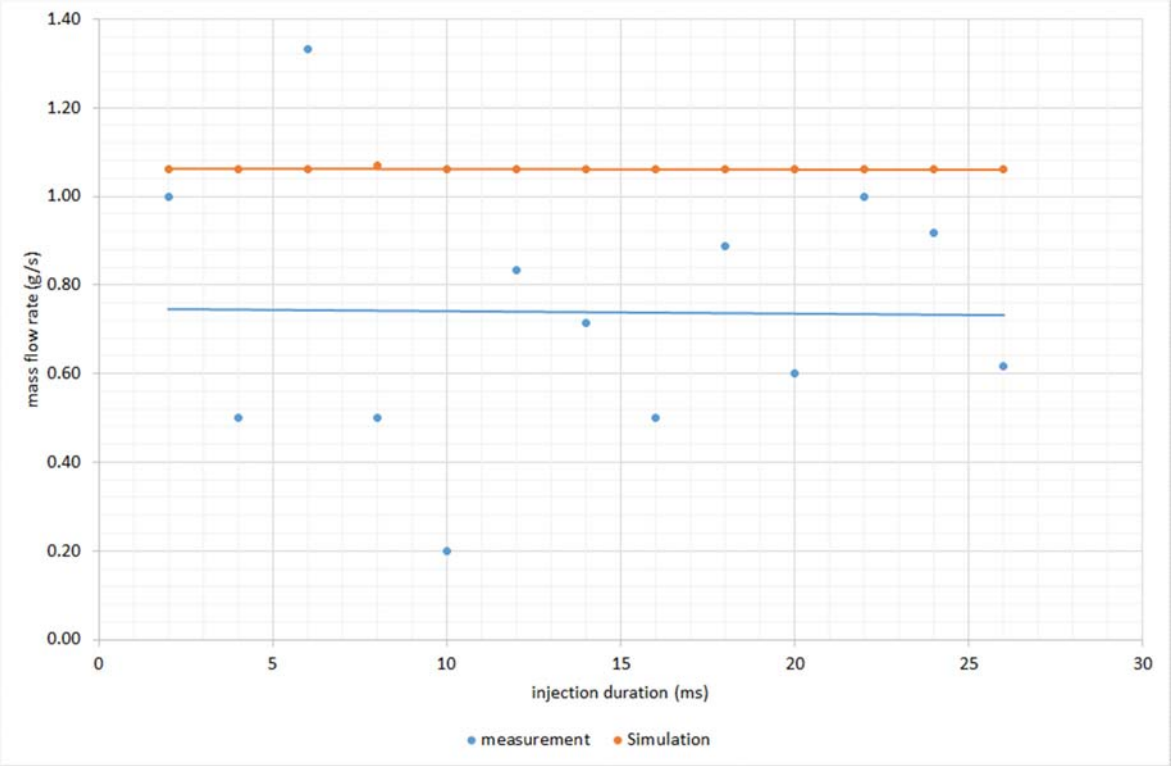

Figure 11. Comparison of measured and simulated of mass flow rate for different injection duration for Case 2.

7. Conclusions

Experimental work has been carried out to describe the jet characteristics of CNG injection for a single-hole direct injector for different injection pressure and injection duration. An analytical model of the injector was also developed to predict the injection mass flow rate. The quantitative results of the injection experiment are useful to understand the characteristics of the injector at different injection pressure. The mass flow rate through the injector is affected by injection pressure linearly as shown in table 4. The mass flow rate is only dependent on upstream pressure because the injector nozzle is operated in chocked condition. It was also shown by Case 2 that average mass flow rate at short injection duration is lower than recorded data in Case 1 of 50 bar injection pressure eventhough the range of the resultant mass flow rate is comparable to each other. The injection pressure of 50 bar is used as the baseline case for Case 2. The deviation is due to the fluctuating mass flow rate data produced for Case 2. We believed that that the fluctuating values of the mass flow rate at short injection duration is due to the internal losses of the injector. The internal losses are hydraulic and electrical losses as well as the hysteresis (magnetic and hydraulic) of the electromagnetic material. Based on simulation results, the analytical model of the injector are able to predict the trend of the injector mass flow rate at different injection pressure and different injection duration. However, the fluctuated trend of experimental data in Case 2 were unable to be predicted by the model.

Acknowledgments

The present research activity has been carried out as part of the CNG Direct Injection Project of the Universiti Malaysia Pahang. The authors would like to thank the technical staff of Automotive Laboratory of Automotive Engineering Centre (AEC) of Universiti Malaysia Pahang, members of Innovative Manufacturing and Mechatronics (IMAMS) laboratory, Faculty of Manufacturing Engineering, Universiti Malaysia Pahang, Malaysia. Moreover, finally to Universiti Malaysia Pahang for providing the funding for the project under short grant scheme.

References

[1] Pourkhesalian A M, Shamekhi, A H, and Salimi, F 2010 Alternative fuel and gasoline in an SI engine: A comparative study of performance and emissions characteristics *J. Fuel* **89** 5 p 1056-1063
[2] Cho H M and He, B Q 2007 Spark ignition natural gas engines-A review *J. Energy Conversion and Management* **48** 2 p 608-618
[3] Sen A K, Zheng, J, and Huang, Z 2011 Dynamics of cycle-to-cycle variations in a natural gas direct-injection spark-ignition engine *J. Applied Energy* **88** 7 p 2324-2334
[4] Kalam M A and Masjuki, H H 2011 An experimental investigation of high performance natural gas engine with direct injection *J. Energy* **36** 5 p 3563-3571
[5] Ouellette P, Mtui, P L, and Hill, P G 1998 Numerical Simulations of Directly Injected Natural Gas and Pilot Diesel Fuel in a Two-Stroke Compression Ignition Engine *J. Sae Technical Paper Series* 724
[6] Banapurmath N R, Tewari, P G, and Hosmath, R S 2008 Experimental investigations of a four-stroke single cylinder direct injection diesel engine operated on dual fuel mode with producer gas as inducted fuel and Honge oil and its methyl ester (HOME) as injected fuels *J. Renewable Energy* **33** 9 p 2007-2018
[7] Carlucci A P, de Risi, A, Laforgia, D, and Naccarato, F 2008 Experimental investigation and combustion analysis of a direct injection dual-fuel diesel-natural gas engine *J. Energy* **33** 2 p 256-263
[8] Gebert N, Beck, R, Barkhimer, H, and Wong, A K. Wells, Development of pilot fuel injection system for CNG engine, Diesel Engine *J.* **2012** 1996 SRC - GoogleScholar p 12-04
[9] Hodgins K B, Hill, P G, Ouellette, P, and Hung, P 1996 Directly Injected Natural Gas Fueling of Diesel Engines *J. Sae Technical Paper Series*
[10] Papagiannakis R G, Rakopoulos, C D, Hountalas, D T, and Rakopoulos, D C 2010 Emission characteristics of high speed, dual fuel, compression ignition engine operating in a wide range of natural gas/diesel fuel proportions *J. Fuel* **89** 7 p 1397-1406
[11] Chiodi M, Berner, H-J, and Bargende, M 2006 Investigation on different Injection Strategies in a Direct-Injected Turbocharged CNG-Engine *J. SAE Technical Paper*
[12] Mohamad T, Harrison, M, Jermy, M, and How, H 2010 The structure of the high-pressure gas jet from a spark plug fuel injector for direct fuel injection *J. Journal of Visualization* **13** 2 p 121-131
[13] Chan E C, Evans, R L, Davy, M H, and Cordiner, S 2007 Pre-ignition characterization of partially-stratified natural gas injection *J. SAE Technical Paper*
[14] Petersen B R, 2006 Transient high-pressure hydrogen jet measurements [Ph.D. thesis]. University of Wisconsin
[15] Chitsaz I, Saidi, M H, Mozafari, A A, and Hajialimohammadi, A 2013 Experimental and numerical investigation on the jet characteristics of spark ignition direct injection gaseous injector *J.* **105** p 8-16
[16] Hajialimohammadi A, Honnery, D, Abdullah, A, and Mirsalim, M A 2013 Time resolved characteristics of gaseous jet injected by a group-hole nozzle *J.* **113** p 497-505
[17] Hill P G and Ouellette, P 1999 Transient Turbulent Gaseous Fuel Jets for Diesel Engines *J. Journal of Fluids Engineering* **121** 1 p 93-101
[18] Abraham J 1996/09/01 1996 Entrapment Characteristics Of Transient Gas Jets *J. Numerical Heat Transfer, Part A: Applications* **30** 4 p 347-364
[19] Ouellette P and Hill, P G 1999 Turbulent Transient Gas Injections *J. Journal of Fluids Engineering* **122** 4 p 743-752
[20] Chitsaz I, Saidi, M H, and Mozafari, A A 2011 Semi Analytical Solution to Transient Start of Weakly Underexpanded Turbulent Jet *J. Journal of Fluids Engineering* **133** 9 p 091204-091204-8
[21] Ouellette P, 1996 Direct injection of natural gas for diesel engine fueling [Ph.D. thesis]. University of British Columbia

[22] Zhang X, Palazzolo, A, Kweon, C-B, Thomas, E, Tucker, R, and Kascak, A 2014 Direct Fuel Injector Power Drive System Optimization *J. SAE Int. J. Engines* **7** 3
[23] Digesu P, Ficarella, A, Laforgia, D, Bruni, G, and Ricco, M 1994 Diesel Electro-injector:A Numerical Simulation Code *J. SAE Technical Paper*
[24] Coppo M, Dongiovanni, C, and Negri, C 2004 Numerical analysis and experimental investigation of a common rail-type diesel injector *J.* **126** 4 p 874-885
[25] Coppo M and Dongiovanni, C 2007 Experimental validation of a common-rail injector model in the whole operation field *J.* **129** 2 p 596-608
[26] Digesu P, Ficarella, A, Laforgia, D, Bruni, G, and Ricco, M 1994 Diesel Electro-injector:A Numerical Simulation Code *J. SAE Technical Paper*
[27] Ficarella A and Laforgia, D 1998 Experimental and Numerical Investigation on Cavitating Flows in Diesel Injection Systems *J. Meccanica* **33** 4 p 407-425
[28] Hu Q, Wu, S F, Stottler, S, and Raghupathi, R 2001 Modelling of Dynamic Responses of an Automotive Fuel Rail System, Part I: Injector *J. Journal of Sound and Vibration* **245** 5 p 801-814
[29] Ando R, Koizumi, M, and Ishikawa, T 2001 Development of a simulation method for dynamic characteristics of fuel injector *J. Magnetics, IEEE Transactions on* **37** 5 p 3715-3718
[30] Tsai W C and Yu, P C 2011 Design of the Electrical Drive for the High-Pressure GDI Injector in a 500cc Motorbike Engine *J. International Journal of Engineering and Industries* **2** 1 p 70-83
[31] Erfan I, Chitsaz, I, Ziabasharhagh, M, Hajialimohammadi, A, and Fleck, B 2015 Injection characteristics of gaseous jet injected by a single-hole nozzle direct injector *J. Fuel* **160** p 24-34
[32] Schimpf P H 2013 A Detailed Explanation of Solenoid Force *J. Int. J. on Recent Trends in Engineering and Technology* **8** 2
[33] Antunes J M G, 2010 The Use Of Hydrogen As A Fuel For Compression Ignition Engines Phd School of Marine Science and Technology Newcastle University England.